Journal Pre-proof

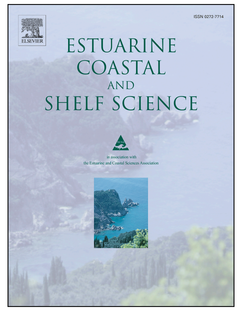

Morphological characterization of ponds and tidal courses in coastal wetlands using Google Earth imagery

G. Noelia Revollo Sarmiento, Natalia V. Revollo Sarmiento, ClaudioA. Delrieux, Gerardo M.E. Perillo

PII: S0272-7714(20)30772-1

DOI: https://doi.org/10.1016/j.ecss.2020.107041

Reference: YECSS 107041

To appear in: *Estuarine, Coastal and Shelf Science*

Received Date: 31 July 2019

Revised Date: 9 August 2020

Accepted Date: 29 September 2020

Morphological Characterization of Ponds and Tidal courses in Coastal Wetlands using Google Earth Imagery

G. Noelia. REVOLLO SARMIENTO[a,*], Natalia V. REVOLLO SARMIENTO[b], Claudio. A. DELRIEUX[a], Gerardo M. E. PERILLO[c,d]

[a]*Dpto. de Ing. Eléctrica y de Computadoras, UNS-CONICET. Avenida Alem 1253, 8000 Bahía Blanca, Argentina*
[b]*Instituto de Investigaciones en Ingeniería Eléctrica and Dpto. de Ing. Eléctrica y de Computadoras,UNS-CONICET. Avenida Alem 1253. Bahía Blanca, Argentina*
[c]*Instituto Argentino de Oceanografía, CONICET-UNS. CC 804, B8000FWB. Bahía Blanca, Argentina*
[d]*Departamento de Geología, UNS. San Juan 670. Bahía Blanca, Argentina*

Abstract

Ponds and tidal courses are significant landforms that frequently arise in marshes and tidal flats environments. An understanding of their development and permanence is relevant to determine future dynamic processes that alter tidal flats and salt marshes environments, such as changes in the sea level, increase in the wave activity, and some other variations associated to the climate change. Direct access for monitoring in these regions is complex, extremely expensive and not always feasible. Remote sensing imagery represents a monitoring alternative, but requires the research of specific image processing procedures to extract the information concerning to these environmental studies. In this work, we developed a methodology for assessing the relevant morphological parameters of ponds and tidal courses using Google Earth imagery. An automatic classifier identifies these landforms as such (accuracy over 86 %), producing a shape descriptors dataset. Then, ponds and tidal courses in tidal flats are morphologically characterized, and their behavior is compared to the surrounding environment. Subsequent analysis found significant differences in morphological characteristics that arise independently of the marsh environmental conditions. The evidence suggests that the evolution processes of the depressions in salt flat environments are clearly different in comparison with salt marshes environments. In salt marshes, the permanence and evolution of the depressions is related to the age of marshes, whereas in tidal flats the dynamic processes and sediment input have influence on depressions evolution.

Keywords: ponds; tidal courses; digital image processing; classification; shape descriptors.

1 Introduction

Estuary systems are one of the most productive ecosystems in the planet. They are subject to diverse processes (i.e., geomorphological, physical, biological, hydrological, ecological, among others). Tidal flats and salt marshes are typical coastal environments that are morphologically similar, but differ according to the presence or absence of halophytic vascular vegetation (Perillo et al., 2001; Ginsberg and Perillo, 2004). Tidal flats generally present a low relief topography and are found in low areas directly influenced by the tides. Tidal propagation, waves, wind, rain and evaporation are dynamic factors that play an important role in the origin and development of different landforms common in tidal environments, such as ponds and tidal courses (Chapman, 1960; Perillo, 2009). Ponds are depressions on tidal flats or marsh surface where water may or may not be retained after tidal inundation (Perillo and Iribarne, 2003; Perillo, 2019). In this paper we will be concerned only with 'ponds' as intertidal depressions with areas between 2 and 20 m^2 and a maximum depth of 50 cm that

*Corresponding author. Tel./fax: +54291 486 1112/1519/1309. Current address: CC804, B8000FWB. Bahía Blanca, Argentina.

Email addresses: giselarevollo@gmail.com (G. Noelia. REVOLLO SARMIENTO), revollonatalia@gmail.com (Natalia V. REVOLLO SARMIENTO), cad@uns.edu.ar (Claudio. A. DELRIEUX), gmeperillo@criba.edu.ar(Gerardo M. E. PERILLO)

preserve water during the whole tidal cycle except in regions with high evaporation (Perillo, 2019).

In the fields of morphodynamics and morphology of coastal environments, the analysis of ponds is of great interest, since they are an integral part of the biological processes such as the infauna habitat, bird feeding, etc. (Perillo, 2009, 2019). Furthermore, this understanding is essential for the management of restoration sites in coastal wetlands (Brand et al., 2012; Shih et al., 2015). Notwithstanding their importance, detailed geomorphologic studies of ponds in tidal flat environments are scarce (Revollo Sarmiento et al., 2016). Systematic observations performed by Perillo (2019) in the flats of the Bahía Blanca Estuary (Argentina) show evident differences between marsh and tidal flats as regards the formation, classification and interaction mechanisms. For the purpose of the present paper, we only consider tidal depressions falling into the pond category defined above.

The study of ponds formation was pioneered by Yapp et al. (1917), who typified them morphologically into two types: primary (barely circular depressions) and secondary (longer and more winding courses). According to current theories in the literature, primary ponds are formed in the marshes' first stages of development (Steers, 1964; Pestrong, 1965; Verger, 1968), whereas secondary ponds are formed in fully developed marshes (Packham and Liddle, 1970; Pethick, 1974; Perillo and Iribarne, 2003). Considering theories from several authors (Boston, 1983; Frey, 1985; Perillo and Iribarne, 2003; Escapa et al., 2015), Perillo (2019) proposed that ponds are formed by three different mechanisms: a) dynamical, b) geomorphological, and c) biological. Dynamical mechanisms are related to the action of waves, water currents, climatic factors that rework the surface. Geomorphologic mechanisms refer to closure or expansion of parts of tidal courses, like sediment compaction or levee formation, among others. Biological mechanisms include plant avoidance, active burrowing by crabs, etc.

The characterization of ponds is commonly performed through measurements taken *in situ*. The typical parameters are area, perimeter, largest diameter, depth and also other shape descriptors such as form factor, roundness, etc. This process involves a significant burden, including i) limited access whether by sea or by land due to regular tidal flooding, ii) high transportation cost and time, and iii) a negative environmental impact of measurement campaigns. Indeed, direct access to the study area alters the natural state of depressions and the surrounding environment, which prevents an unbiased analysis of their future evolution.

Remote sensing allows high scale geographical and temporal studies without altering the natural state of the subject matter (Revollo et al., 2016; Ijaz et al., 2018) and currently is widely used to perform analyses in areas such as biotechnology, precission agriculture, and earth sciences (Wang et al., 2017; Rishikeshan and Ramesh, 2017; Belgiu and Csillik, 2018). This technology encompasses several challenges in the analysis of small landforms (m to cm) arising in coastal environments. Freely available satellite imagery (i.e., LANDSAT) lacks the resolution to identify these features (30 m resolution) and higher resolution imagery (i.e., IKONOS) is expensive for geographically extensive studies (Revollo Sarmiento et al., 2016; Tatar et al., 2018). Indeed, applying different techniques to improve the free available images resolution

(Cipolletti et al., 2012, 2014) is not enough to identify different sizes of ponds. Google Earth (GE), in turn, is a powerful information source that can be used for a variety of purposes and has enabled innovative research in Earth Sciences (Goudie, 2013; Gorelick et al., 2017).

The aim of this work is the morphological characterization of ponds and tidal courses and their variations in tidal flat environments using GE images. We applied the methodology to the extensive tidal flats of the Bahía Blanca Estuary, which has very large fields of ponds widely distributed.

2 Materials and Methods

2.1 Selection of study areas

Fourteen tidal flat sites with all possible varied morphological characteristics of ponds and tidal courses (sizes, shapes and orientations) were selected (Table 1). According to the surface morphology, these sites (Fig. 1) are located between the internal and the middle sector of the Bahía Blanca Estuary (Perillo and Piccolo, 1999). The total surface of the estuary is bounded in approximately 2300 km^2, corresponding only 410 km^2 to islands, the intertidal sector covers 1150 km^2 whereas the subtidal one is 740 km^2. The total area of the present study covers approximately 1503 km^2 and comprises almost 79.5 % of the total surface of the tidal flats in the Bahía Blanca Estuary (Perillo and Piccolo, 1999). Mean tidal range in the estuary varies from 2.2 m at the mouth to 4m at the head (Perillo and Piccolo, 1991) The differences between spring and neap levels is about 0.50 to 1 m. Unfortunately all tidal stations are located along the northern coast of the Canal Principal and the degree of flooding of the tidal flats can be inferred only from estimations made by researchers at Instituto Argentino de

Oceanograf´ıa (IADO) and sailors, during surveys that are carried out periodically since more than 50 years. In all cases the reports coincide that most of the intertidal areas are covered by about 0.5 to 1.5 m of water, although there are no adequate mapping of these floodings. When measured, maximum tidal currents on the tidal flats are on the order of 0.5 m/s (Pratolongo et al., 2010). Wind is a major dynamic component of the estuary with average speed of the order of 18 km/h but often reaching value of over 40 to 70 km/h. More than 40 % of the time wind blows from the NW and N being less frequent from the SW and SE (Piccolo et al., 1989).

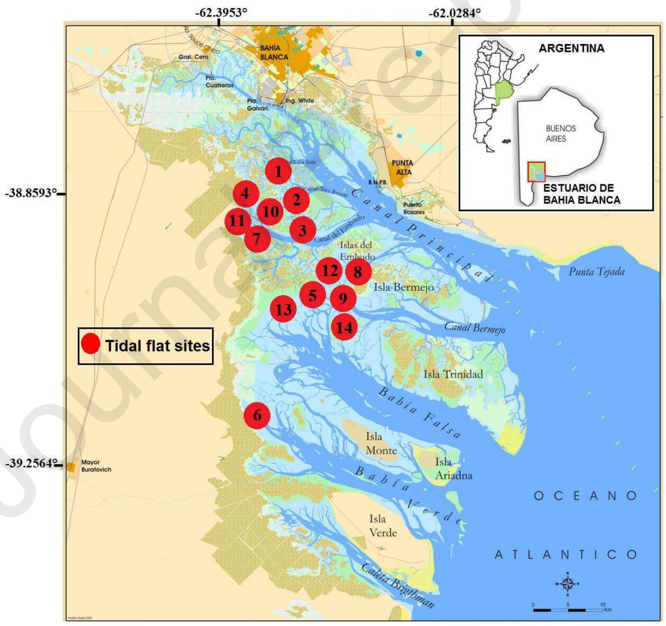

Fig. 1. Bahía Blanca Estuary, distribution of tidal flat study sites (in red).

Table 1. Geographic location of the study areas and acquisition date.

Sites	Latitude (S)	Longitude (W)	Acquisition date
Sites 1	−38.898074°	−62.271961°	12/26/2012
Sites 2	−38.901586°	−62.220930°	12/26/2012
Sites 3	−38.959019°	−62.226407°	12/26/2012
Sites 4	−38.914293°	−62.321013°	12/26/2012
Sites 5	−39.008280°	−62.192548°	03/18/2011
Sites 6	−39.212749°	−62.300189°	03/18/2011
Sites 7	−38.952229°	−62.311871°	12/26/2012
Sites 8	−39.001640°	−62.144144°	03/18/2011
Sites 9a	−39.002303°	−62.144591°	03/18/2011
Sites 9b	−39.019532°	−62.161046°	03/18/2011
Sites 10	−38.917989°	−62.315777°	12/26/2012
Sites 11	−38.946148°	−62.334869°	12/26/2012
Sites 12	−39.002224°	−62.182938°	12/26/2012
Sites 13	−39.032259°	−62.212384°	12/26/2012
Sites 14a	−39.003146°	−62.143629°	03/18/2011
Sites 14b	−39.020109°	−62.163469°	03/18/2011

GE images provide a wide spatial coverage, at the same time, enough spatial resolution because it maps the Earth by superimposing satellite images from different spatial missions (i.e., Landsat8, Spot 6/7, Ikonos, GeoEye, WorldView, etc.) and aerial photography. GE imagery resolution ranges from 15 m of resolution to 15 cm. This spatial resolution allows to establish accurate and precise individual measurements using specifically developed image processing algorithms, despite some limitations (i.e., images have only three visible spectral bands, and low revisit rate in many regions worldwide). Also there are other similar tools such as Bing Maps and Apple Maps that deliver high resolution imagery. GE, however, is still unique in the sense that it provides the time line search feature, which for this research is required to be able to perform geomorphological studies involving the target landforms: ponds and tidal courses in tidal flats, considering that the images of this tidal zones should match with low tide moments.

Twenty-four 1290 × 496 pixel GE frames were used to analyze the tidal flats. These frames were exported from GE application (version 5.2.1.1588) as images in RGB format with their corresponding spatial reference. The virtual altitude (eye alt) of the frames was set to 290 m, corresponding to a geographic extent of 360 × 174 m per frame. The scale at this altitude in GE is 64 m and it is consistent with the required spatial resolution (~30 cm/pixel), allowing measurements with an appropriate accuracy and precision to make reasonable comparison among sites. Different factors were considered during image selection, including the time of day in which the satellite captured the image (dark areas in a visible satellite image represent geographic regions where only small amounts of visible sunlight are reflected back to space), the tidal status, and other weather conditions such as clouds. Given the image records offered by GE, the images selected were the ones obtained on March 18, 2011 and December 26, 2012 due to these two timeline images consider the factors mentioned above (Table 1).

2.2 Processing, Measurement and Computation of Morphological Descriptors

The images were segmented into foreground (ponds, tidal courses, others landforms) and background pixels (not landforms) using a 'multi-distance' algorithm (Revollo Sarmiento et al., 2016). After this procedure, every connected set of foreground pixels was candidate to be identified either as pertaining to a pond, a tidal course, or to other spurious landforms (Fig. 2). An unsupervised classifier and a set of shape descriptors (dimensionless values) introduced by Revollo Sarmiento et al. (2016) were computed in all sites of the estuary. The shape descriptors proposed in prior works (Revollo Sarmiento et al., 2016) were the minimax rectangular box area (*abox*), form factor (*ff*), Feret's diameters with modulus and angles (F_{max}, F_{min}), extension (*ext*), and compactness (*cp*). However, to get a complete morphological characterization, an additional set of new shape descriptors was computed. In this context, five shape descriptors were selected for a better shape characterization: roundness (*rd*), aspect ratio (*ar*), elongation (*elg*), curl (*cr*), and net area-main diagonal relationship (*amd*) (Russ, 1999) (Table 2). These modifications were introduced in a new version of the developed software using Qt Creator IDE and OpenCV (Open Source Computer Vision Library). However, the processing methodology can easily be developed in other software platforms (i.e., Python, Matlab, Delphi, Java, etc).

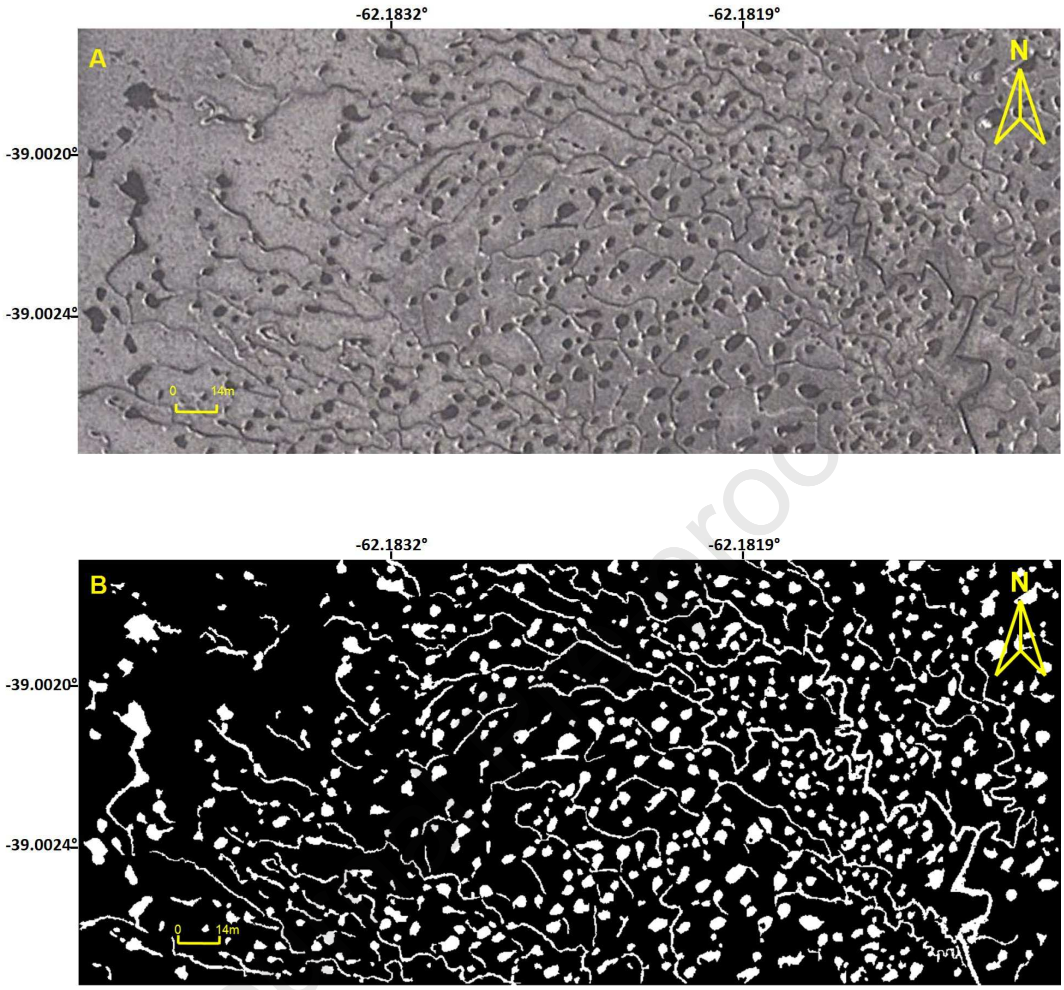

184 Fig. 2. Site 12 in the Bahía Blanca Estuary. (A) Original GE image. (B) Binary
185 image (foreground pixels in white representing ponds and tidal courses).

Table 2. Shape descriptors and their mathematical definition.

Name	Symbol	Math Definition
Roundness	*rd*	$\frac{4A}{\pi F_{\text{máx}}^{2}}$
Aspect Ratio	*ar*	$\frac{F_{\text{máx}}}{F_{\text{miın}}}$
Elongation	*elg*	$\frac{L}{W}$
Curl	*cr*	$\frac{F_{\text{máx}}}{L}$
Amd	*amd*	$\frac{A_{net}}{F_{\text{máx}}}$

Form factor (*ff*) formally describes the deviation of the perimeter of a given shape with respect to the perimeter of an ideal circle of equivalent area. However, several rather different shapes may have the same *ff* (Fig. 4A).

Roundness (*rd*) also measures how a shape deviates from an ideal circle, but in terms of the relationship between area and diameter. In this regard, these two descriptors (*ff* and *rd*) are able to distinguish different shapes more precisely. Feret's diameters (F_{max} and F_{min}) are the largest and smallest distances arising between two parallel lines tangent to the shape (Feret, 1931). A quick although accurate measurement can be obtained rotating the shape with respect to its centroid and about a significant amount of angles [0, Π]. The discretization of interval is done in steps of Π/180 (1 degree). For each rotation the extension of the shape along a principal axis is measured, and the largest and

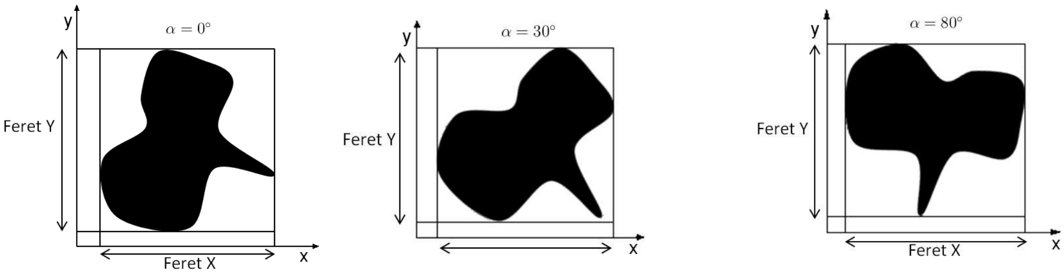

Fig. 3. Maximum and minimum Feret diameter. (A) Feret diameter measurement. (B) Feret diameter for a rotation of 30˚. (C) Feret diameter for a rotation of 80˚.

smallest values are estimations of F_{max} and F_{min}, respectively (Fig. 3). The elongation descriptor (*elg*) measures how long is the shape, computing the fiber length (*L*) and the mean width of the shape (*W*). A prior shape skeletonization is required to compute *L*, using a conditional thinning algorithm, such as proposed by Zhang and Suen (1984). The resulting *L* is measured (Fig. 5A) and, assuming that the shape can be regarded as ribbon with uniform width *W* , net area *A* and length *L*, *W* can be estimated as $W \approx A/L$ (Fig. 5B). The descriptor *elg* is the ratio between *L* and *W*. Finally, curl (*cr*) provides a measure regarding how twisted or arched the shape is. Shapes with greater degree of curl correspond with lower values and vice versa (Fig. 4B).

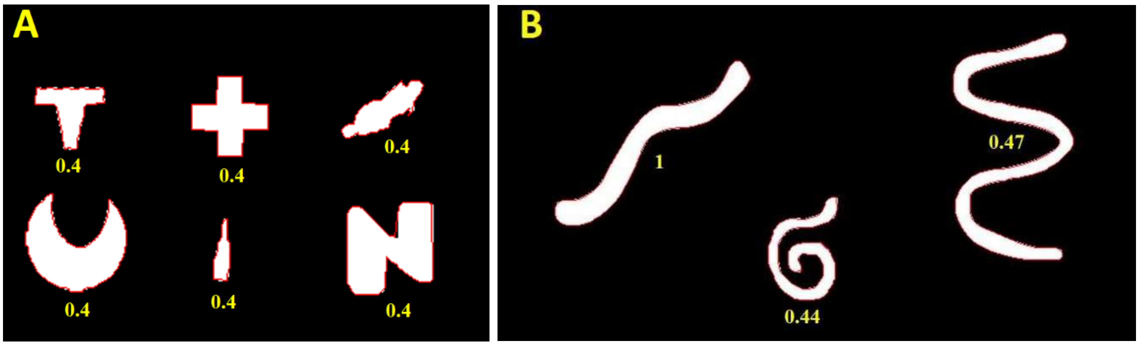

Fig. 4. Shape descriptors. (A) Set of synthetic figures visually different but with identical shape factor values. (B) Set of figures with different curl values (*cr*); *cr* values indicate the curl degree.

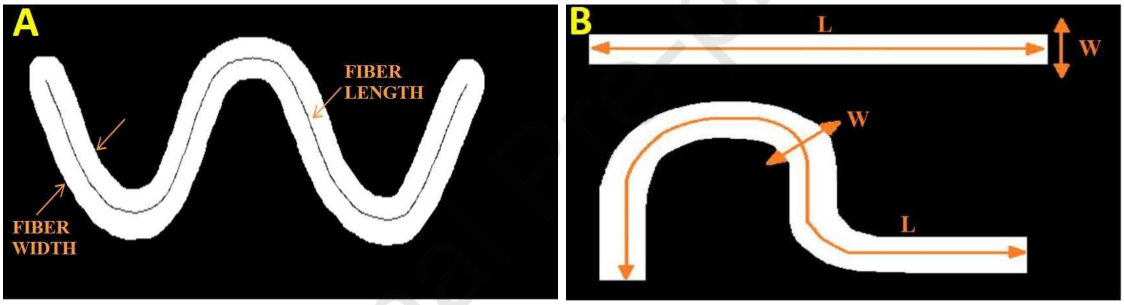

Fig. 5. Elongation shape descriptor. (A) Fiber length and medium width parameters. (B) Geometrical model for a fiber considered as a ribbon length *L* with square endings and a constant medium width *W*.

2.3 Landform Classification and Statistical Analysis

Landforms were classified into three classes: ponds (*P*), tidal courses (*C*), and other structures (*O*) applying the automatic methodological classification proposed by Revollo Sarmiento et al. (2016). In this context, the classifier was applied to all the segmented landforms, and its accuracy was evaluated. The confusion matrix (Congalton and Green, 2008) was computed to analyze the performance of the classifier (Table 3B). Several parameters were calculated from the confusion matrix (Table 3A) to estimate the accuracy of the classifier depending on the total of the studied features (*T*). Cohen's Kappa coefficient (κ) (Cohen, 1960; Wilkinson, 2005) was computed to measure a consensus among automatic classifier and the evaluation of expert geomorphologists. Cohen's κ has become a standard accuracy assessment in the remote sensing literature (Congalton and Green, 2008) despite some criticisms regarding its interpretation (Pontius et al., 2011).

Table 3. Performance matrix. (A) Confusion matrix. (B) Quality standard terms.

A

		Predicted		
		Negative	Positive	Total
Actual	Negative	Tn	Fp	$An = Tn + Fp$
	Positive	Fn	Tp	$Ap = Fn + Tp$
	Total	$Pn = Tn + Fn$	$Pp = Fp + Tp$	T

B

Definition	Symbol	Math Definition
Global Accuracy	A_g	$Tn + Tp/(An + Ap)$
True positive rate	R_{Tp}	Tp/Ap
True negative rate	R_{Tn}	Tn/An
False negative rate	R_{Fn}	Tn/Pn
False positive rate	R_{Fp}	Tp/Pp
Auxiliary parameter	$P_r(a)$	$(Tn + Tp)/T$
Auxiliary parameter	$P_r(e)$	$(An * Pn + Ap * Pp)/T^2$
Cohen's kappa coefficient	κ	$P_r(a) - P_r(e)/(1 - P_r(e))$

An analysis of variance (ANOVA) was performed to explore the variability among different sites. At first, a separate class analysis was performed using the shape descriptors associated to each site. The statistical significance test was based on the Fisher's Test (Fisher's Least Significant Difference) with a significance level $\alpha = 0.05$ (Day and Quinn, 1989). Then, the complete dataset was analyzed using the same strategy.

In each study site, the number of ponds and tidal courses were automatically computed through the processing stage and the density of each class was also computed. The drainage density of courses was estimated as $D_c \approx$ *total length courses* (*km*)/*Area*$_{\text{site}}$ (km^2), considering the sum of *L* as total length courses. The average of area measurements provided information of sites with bigger ponds. Morphologically and according to the criteria of Yapp et al. (1917), it was possible to discriminate between primary and secondary ponds, correlating the values associated to the shape descriptors roundness and aspect ratio. Values closer to one mean that ponds were more likely to be of the primary type (circular), and values closer to zero could represent long ponds. Moreover, the average of these descriptors allowed to appreciate the general shape of ponds in each site, whereas the standard deviation showed the degree of the shape dispersion with respect to the average. Both the elongation and curl of tidal courses were characterized with the corresponding descriptors (*elg* and *curl*), and the maximum length (*TML*) and orientation were derived directly from the Feret's diameters (F_{max} and F_{min}).

3 Results

3.1 Automatic Identification

The methodology for automatic classification introduced by Revollo Sarmiento et al. (2016) was applied in fourteen sites of the estuary of Bahía Blanca and the results were evaluated both quantitatively (model accuracy) and visually (expert knowledge). The classifier accuracy was above 86 % in all sites, being as high as 100 % in site 9. Moreover, sites 12 and 13 have global accuracy (A_g) of 97 (Table 4) and 96 % (Table 5), respectively (Figs. 6 and 7). Despite the high geomorphological variation of these landforms, the results are quite satisfactory, and the global error percentages associated to the study site are in the 5.5 % range (see Fig. 8). The κ value was within the interval [0.7, 0.92] in all sites, which means that the consensus results were optimal.

Table 4. Performance matrix, Site 12. (A) and (B): Confusion matrix and Quality standard terms in site 12a. (C) and (D): Confusion matrix and Quality standard terms in site 12b.

A

		Predicted		
		P	C	O
Actual	P	570	5	6
	C	0	54	0
	O	6	0	59

B

Parameter	Value
A_g[%]	97.57
R_{Tp}	0.98
R_{Tc}	1.00
R_{To}	0.91
R_{Fp}	0.99
R_{Fc}	0.91
R_{Fo}	0.91
$P_r(a)$	0.98
$P_r(e)$	0.70
κ	0.92

C

		Predicted		
		P	C	O
Actual	P	844	1	20
	C	0	48	0
	O	7	1	53

D

Parameter	Value
A_g[%]	97.02
R_{Tp}	0.98
R_{Tc}	1.00
R_{To}	0.87
R_{Fp}	0.99
R_{Fc}	0.96
R_{Fo}	0.72
$P_r(a)$	0.97
$P_r(e)$	0.78
κ	0.86

Table 5. Performance matrix, Site 13. (A) and (B): Confusion matrix and Quality standard terms in site 13a. (C) and (D): Confusion matrix and Quality standard terms in site 13b.

A

		Predicted		
		P	C	O
Actual	P	386	5	7
	C	0	44	0
	O	3	0	51

B

Parameter	Value
A_g[%]	96.98
$R_{T\,p}$	0.97
$R_{T\,c}$	1.00
$R_{T\,o}$	0.94
R_{Fp}	0.99
R_{Fc}	0.90
R_{Fo}	0.88
$P_r(a)$	0.97
$P_r(e)$	0.65
κ	0.91

C

		Predicted		
		P	C	O
Actual	P	284	2	1
	C	0	31	0
	O	10	0	24

D

Parameter	Value
A_g[%]	96.31
$R_{T\,p}$	0.99
$R_{T\,c}$	1.00
$R_{T\,o}$	0.70
R_{Fp}	0.96
R_{Fc}	0.94
R_{Fo}	0.96
$P_r(a)$	0.96
$P_r(e)$	0.70
κ	0.88

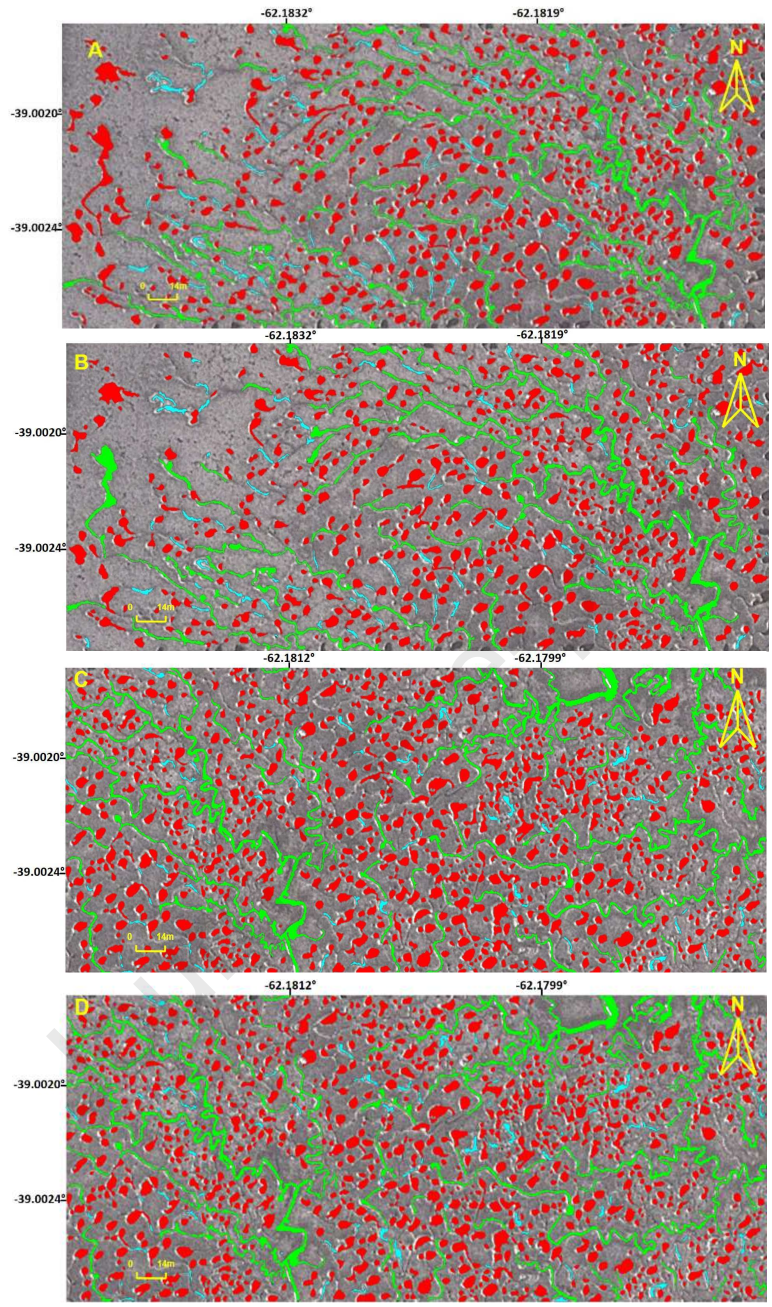

Fig. 6. Classification results in Bah´ıa Blanca Estuary; site 12 with its global precision. (A) Supervised classification Ag = 100 %. (B) Automatic classification Ag = 97.6 %. (C) Supervised classification Ag = 100 %. (D) Automatic classification Ag = 97 %. Ponds, tidal courses and others are shown in red, green, and cyan, respectively.

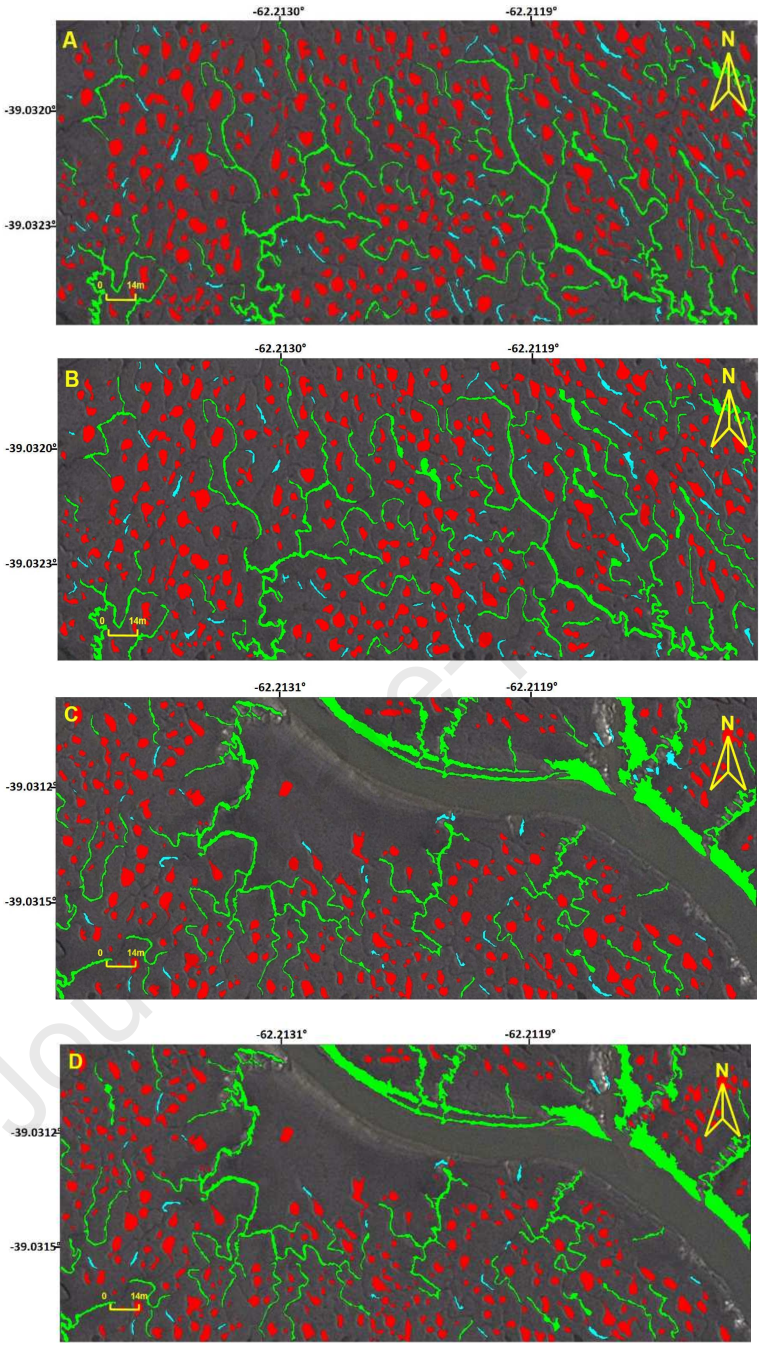

Fig. 7. Classification results in Bahía Blanca Estuary; site 13 with its global precision. (A) Supervised classification Ag = 100 %. (B) Automatic classification Ag = 96.9 %. (C) Supervised classification Ag = 100 %. (D) Automatic classification Ag = 96 %. Ponds, tidal courses and others are shown in red, green, and cyan, respectively.

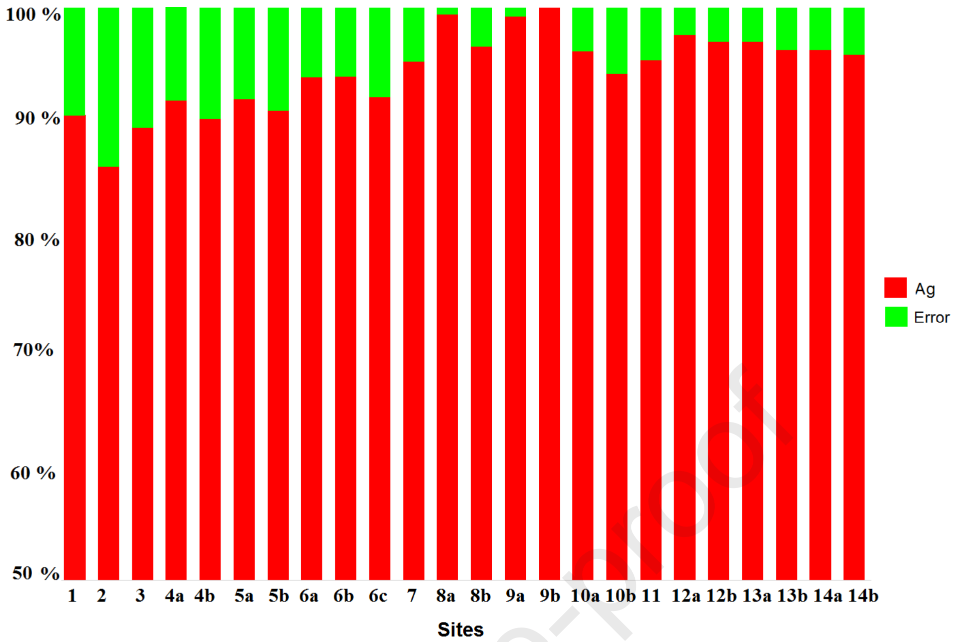

Fig. 8. Accuracy of the automatic classification (red) and its error (green) in each study site.

3.2 Morphological Landforms Characterization

3.2.1. Ponds

The study sites correspond to lower flats in the estuary and Fig. 9A displays the density of ponds distributed in each site. Sites located in the internal zone of the estuary, close to courses Del Embudo and Tres Brazas (sites 2, 3 and 10) presented a higher density of ponds (22 per 100 m^2), whereas the sites closer to courses Bermejo, Paso San Juan and Del Embudo (sites 4, 6, 7, 8, 9, 12, 13 and 14) showed a low density of ponds (7 per 100 m^2). Site 3 presented the highest density, 25 ponds per 100 m^2. The lowest density was located in site 9, 6 ponds per 100 m^2. This site presented a higher number of bigger tidal courses in comparison to other zones.

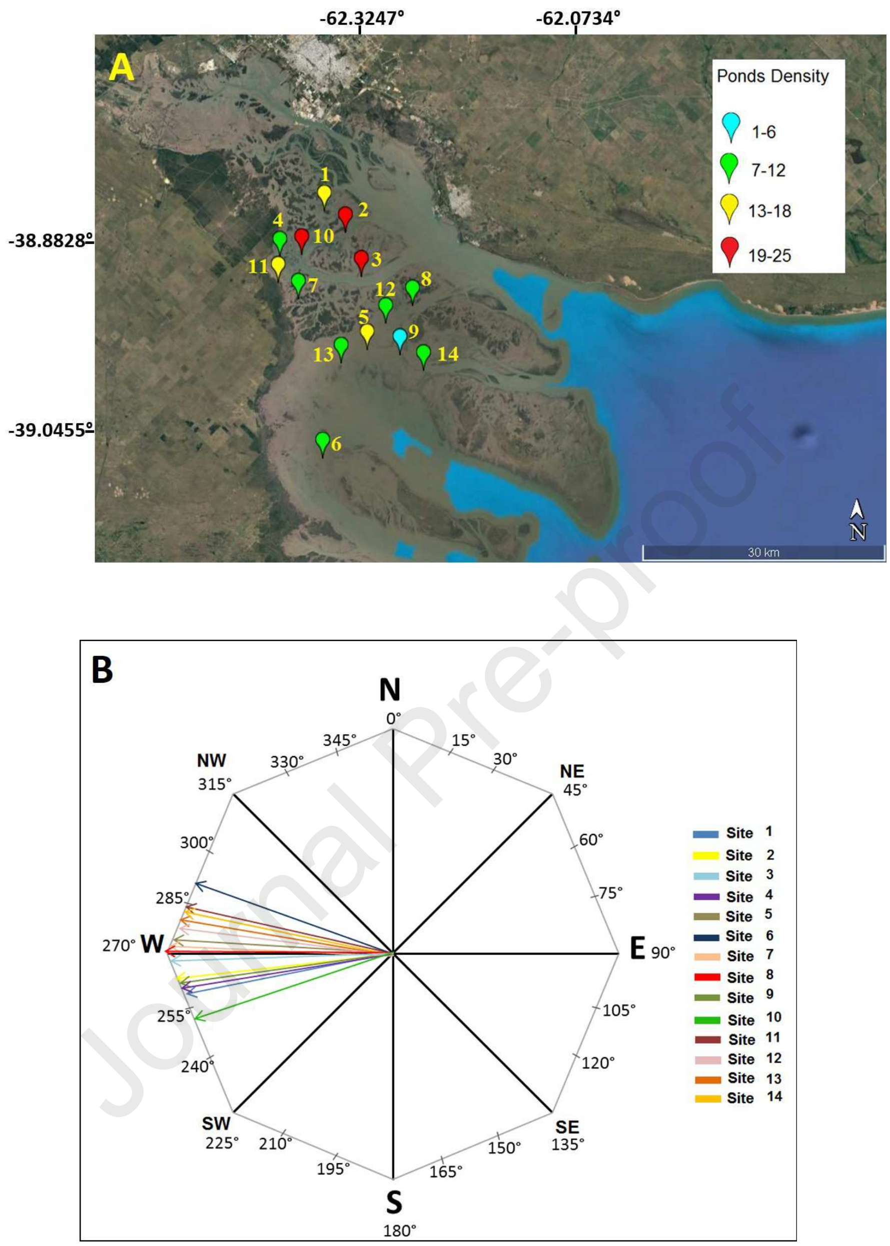

Fig. 9. Ponds density and mean angle orientation per site. (A) Ponds density from low to high values in tidal flats per 100 m^2, in cyan, green, yellow and red. (B) Ponds mean angle orientations.

Post hoc morphometric parameter analyses showed significant differences among sites in the average of the morphological variables (ANOVA, $p < 0.0001$), which were more notorious in sites 3 and 9. Considering size, measured in m^2, sites 3 and 9 were representative of ponds with lowest and highest dimensions (average areas 3.5 and 13 m^2, respectively). In site 3, the lowest and highest sizes of ponds were 0.10 and 24 m^2, whereas in site 9 they were 0.30 and 173 m^2, respectively. Both sites were characterized by numerous big ponds with atypical values. Regarding the shape, the first two main components in principal component analysis explained 98 % of the variance.

The correlation among roundness and aspect ratio ($r = -0.88$), roundness and elongation ($r = -0.81$), and aspect ratio and elongation ($r = 0.58$) were highly significant. Sites 7 and 13 presented a higher number of rounded (primary) ponds, whereas in site 3 these landforms were more elongated (secondary). In site 4, ponds were more symmetrical, characterized by their aspect ratio. Regarding the total maximum length (TML), the minimum and maximum values corresponded to sites 3 and 8 (average values 3 m and 6 m, respectively). The lowest maximum length of the ponds was 0, 14 m, and the highest one 31 m. The orientation angle was directly related to the total maximum length, which was predominant in the N-W and S-W quadrants. In most of the sites, ponds presented orientations in the N-W quadrant and 270° degrees. However, the internal sector sites (1, 2, 3, 4 and 10) and site 9 that is located in the middle region of the estuary contained ponds with orientations between 250° and 270°. Sites 10 and 14 exhibited the maximum and minimum orientations, respectively, with mean angles of 250° and 284° (Fig. 9B).

3.2.2. *Tidal courses*

In general, in all sites, tidal courses are less numerous than ponds so the density of these landforms in tidal flats is very low (Table 6). The highest densities was in sites 2, 5, 8, 12, 13 and 14 (between 0.07 and 0.1 km/km^2), whereas in sites 6 and 7 the presence of tidal courses was zero. The variance analyses showed differences only among elongation, curl, and area parameters (ANOVA, $p < 0.0003$). Regarding size (area), sites 11 and 14 presented tidal courses of lower and higher values (mean area 27 and 577 m^2, respectively). The smallest and biggest tidal course corresponded to areas of 4.3 and 4696 m^2, respectively. Regarding shape, the first two principal components explained 100 % of the variance (elongation and curl). The correlation between both descriptors was (r=−0.46). Considering tidal course length, sites 7 and 11 had the lowest and highest values of elongation coefficients, registering mean values of 30,1 and 88,75, respectively. The total maximum length (TML) lowest and highest values corresponded to sites 7 and 14 with mean values of 22 m and 86 m, respectively. The lowest maximum length of the tidal course was 13,9 m and the highest 209 m. Sites 1, 10 and 9 had tidal courses with the highest and lowest curl, with mean coefficients of 0,5 and 0,6, respectively. The highest and lowest tidal course curl correspond with coefficients of 0,12 and 1,12, respectively. The TML measurements had a predominant orientation towards N-W, S-W quadrants (Fig. 10). Sites 2, 6 and 11 had orientations in S-W quadrant, with mean angles between 250° and 270°. The remaining 11 zones presented orientations in N-W quadrant with mean angles over 275°.

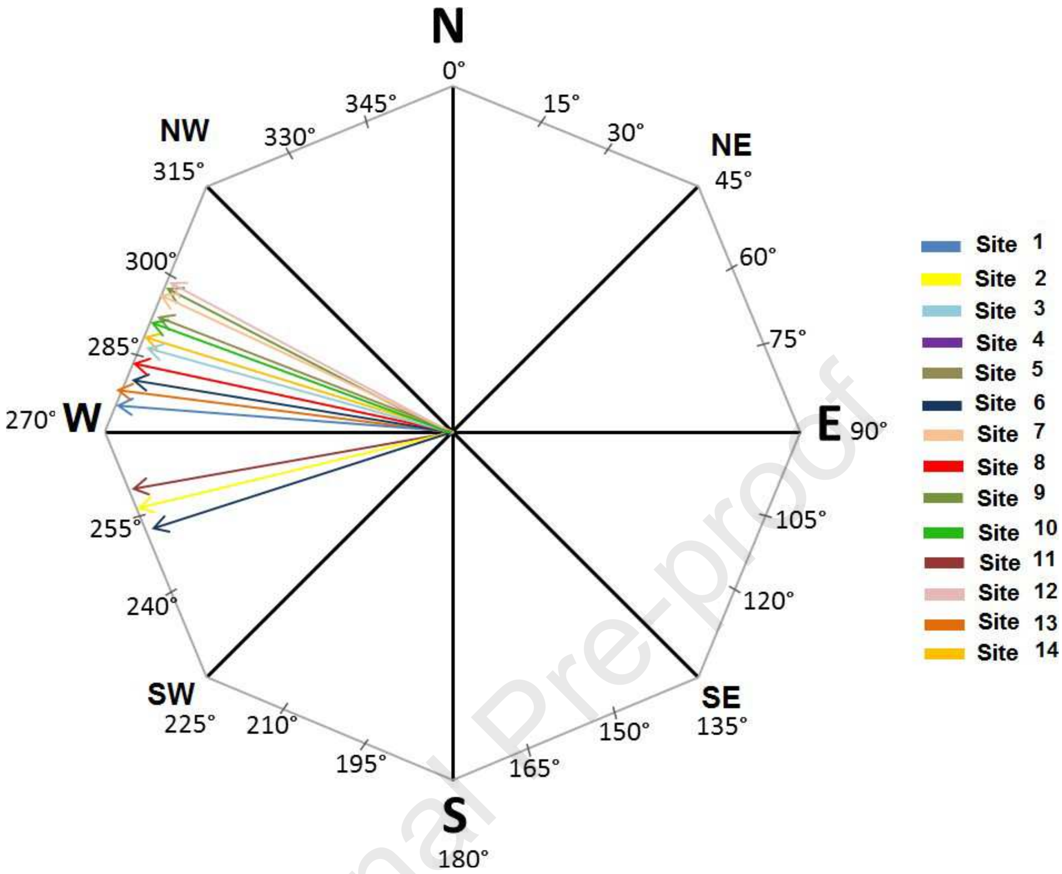

Fig. 10. Tidal courses mean angle orientation per site.

Table 6. Drainage density of courses per site.

Site	D_c (*km/km*^{2})
Zone 1	0.03
Zone 2	0.08
Zone 3	0.04
Zone 4a	0.06
Zone 4b	0.05
Zone 5a	0.1
Zone 5b	0.05
Zone 7	0
Zone 8a	0.07
Zone 8b	0.04
Zone 9a	0.06
Zone 9b	0.05
Zone 10a	0.04
Zone 10b	0.02
Zone 11	0.04
Zone 12a	0.07
Zone 12b	0.10
Zone 13a	0.07
Zone 13b	0.06
Zone 14a	0.05
Zone 14b	0.07

4 Discussion

The automatic classification using specific algorithms of image processing applied to GE images provided a set of data about morphological characteristics of ponds and tidal courses in tidal flat environments. This information allowed to research the variability of the shapes of these geoforms, and their geographical distribution in tidal flats. As compared to *in-situ* measurements, our methodology required considerably less time and lower costs, and the amount and quality of the gathered information is remarkably higher.

The accuracy of the automatic classifier massively applied in tidal flat areas was high (A_g over 86 %), with a consensus measurement compared to the manual classification for all zones (κ-index over 0.8). Morphological data analysis of ponds evidenced remarkable differences in relation to the mechanisms of their formation and evolution between marsh and tidal flat environments. According to different theories and from the morphological point of view proposed by Yapp et al. (1917), primary ponds are formed in the first stages of marsh development, whereas the secondary ones are originated as marshes mature. This process was different in ponds formed in tidal flat environments, because it was possible to distinguish according to their shape between primary and secondary ponds in mature flats. Sites located in the internal sector of the estuary presented the highest density of ponds, due to the constant flooding of flats given their low slopes and high drainage net (Melo, 2004; Melo and Perillo, 2006; Piccolo et al., 2008). Sites in the middle sector of the estuary had low density of ponds, and however they presented more tidal courses.

According to the theory proposed by Boston (1983), densities should be higher in zones with little flooding, which allows a higher persistence of ponds. However, Boston's theory is not consistent with our results, where high densities are in low slope flats with constant flooding. The main difference with Boston's theory is that his work refer to vegetated environments which have completely different behavior than denuded tidal flats as in our research. Most of the tidal flats in Bahía Blanca are low flats, being inundated about 730 times per year (Perillo and Piccolo, 1999). Therefore, they are subject to constant dynamic processes which are not regulated by the presence of significant vegetation. Furthermore, the extensive network of large tidal courses (courses and creeks) provide the means for the frequent flooding of the studied areas. In essence, depressions in marshes and tidal flats clearly have different evolution processes. As indicated by Perillo (2019) marsh depressions, in many cases, have been inherited from the previous tidal flats. Their persistence and evolution depends on the sediment input into the marsh, dynamic processes (waves, tides, currents, etc.) and the vegetation dynamics. Whereas, in tidal flats, except for the influence of the infauna, the evolution of the depressions is only affected by the dynamic processes and sediment input. In the particular case of Bahia Blanca Estuary, which is sediment starved (Perillo and Piccolo, 1999), the most important factors are the dynamic.

Several authors agree that ponds and tidal courses densities are inversely related. If tidal courses density is higher than ponds density, ponds probability to drain or to be covered by vegetation, in the case of marshes, is also higher (Packham and Liddle, 1970; Pethick, 1974). In our case, tidal courses density was low in all sites and the sediment provision was also low. The Bahia Blanca Estuary is a former delta that presently has neither major sediment input from the continent nor from the sea. Most of the suspended sediment is provided by the direct erosion of the intertidal areas by tidal currents and intense locally-generated wind waves (Perillo et al., 2001). Therefore, the formation of the ponds is most likely due to dynamic processes as proposed by Perillo (2019). Moreover, we observed that ponds density change in time, increasing and diminishing regardless of the flat age. This observation was confirmed by means of temporal analyses of ponds distribution using the image record of the GE application (Fig. 11).

Zones with higher density of ponds also have bigger ponds, so size of ponds seemed to be related with their density in a determined region. In the internal region of the estuary, zones 3, 4 and 7, have longer, more symmetric, and more round ponds, respectively. These zones had the maximum tidal range, which suggest that the currents are more significant in the last periods of reflux. This drives the primary ponds to become longer or to join together, forming secondary ponds. Wind is also other factor of influence, landforms have general angles coincident with the dominant N-W wind direction. Even though there is not conclusive data to relate the morphological variables with other environmental factors (e.g., stream-flow, tidal flat age, erosion level, relative changes in the sea level, wind speed, precipitation, humidity rates), the presented results allow us to state that the influence of these factors is relevant in the formation and evolution of these landforms in tidal flat environments.

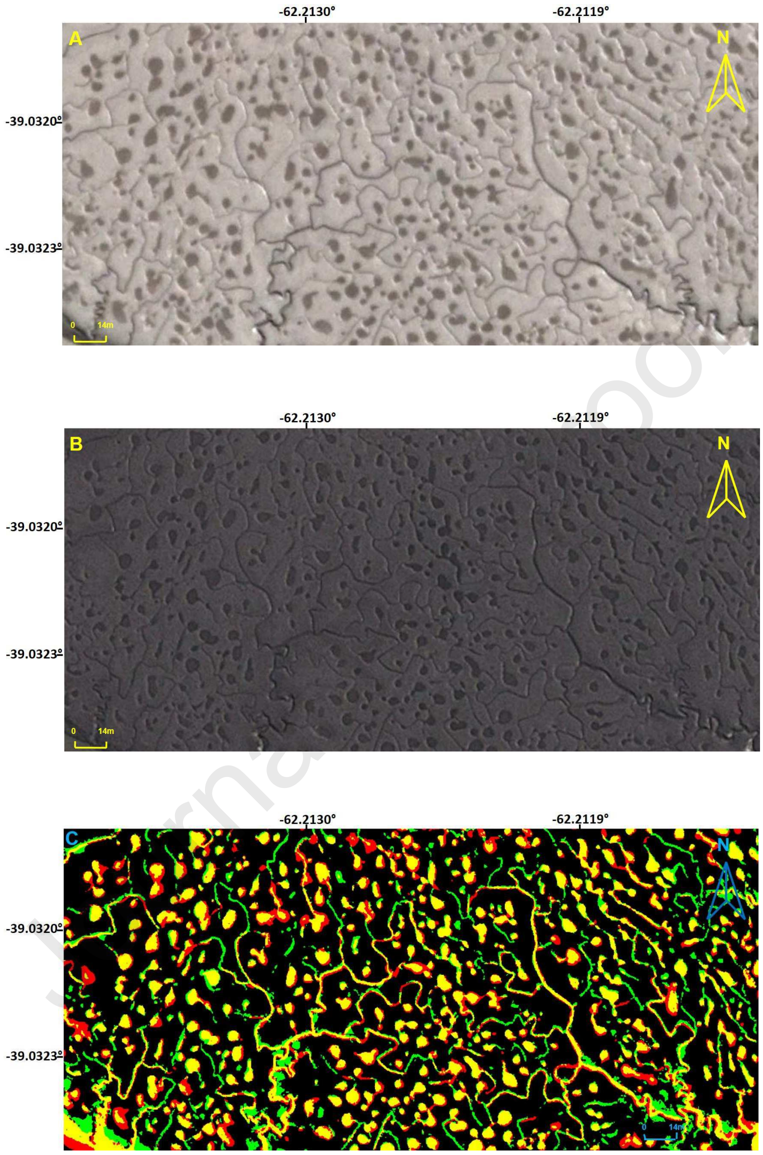

Fig. 11. Variation in size and form of landforms over time in site 13. (A) Date of acquisition - March 19, 2011. (B) Date of acquisition - December 12, 2012. (C) Merge of thresholded images, years 2011 (red foreground pixels) and 2012 (green foreground pixels), respectively. Yellow foreground pixels represent ponds and tidal courses without variation.

5 Conclusion

We presented a methodology for assessing relevant morphological parameters of ponds and tidal courses using Google Earth imagery. As an expansion of prior research (Revollo Sarmiento et al., 2016), we introduced new shape descriptors in the development of an automatic classifier, which identifies ponds and tidal courses morphology in coastal wetlands with very high accuracy. Fourteen sites were studied within the Bahía Blanca Estuary, covering almost 80% of the total area. The evidence suggests that ponds densities tend to be higher in the internal region of the estuary, a region of constant flooding where the tidal range is maximum. In these zones also the longest, most symmetrical, and most rounded ponds were located. A likely explanation of this observation is that the continuous flooding in low flats contributed to higher densities that play a role in the size and shape of ponds. Considering the type of sediment of tidal flats in the estuary, no differences were found in the densities, because tidal flats were dominated by silty clay. In general, the densities of tidal courses located over the flats were not high in the whole study site, being only higher in areas of permanent flooding. In this context, notorious differences were observed in the formation mechanisms of geoforms in marshes and tidal flats. These results over tidal flats differ from the theories proposed in Boston (1983), according to which, ponds and tidal courses have a higher probability of persistence associated to a high density if they were developed in areas with low flooding, and that high densities were directly related to the marsh age. We also highlighted the importance of wind as a main influence in ponds and tidal courses development considering that the main geoforms orientation agree with the dominant winds.

This methodology enables and complements other research lines, such as a temporal evolution study (geomorphological analysis). Comparing the evolution of these geoforms in recent years will allow to identify the dynamic processes that has influence in different environments, such as tidal flats and tidal marshes. This evaluation, together with other environmental data (i.e., current flow, tidal flat ages, level of erosion, relative changes in sea levels, wind speed, rainfall, etc.) would complement the morphological characterization presented here, providing further understanding of the behavior of these geoforms in its own environment. In this research aim, we are currently carrying out surveys of ponds to correlate *in situ* information with the data gathered by remote sensing techniques.

Acknowledgements

Partial financial support for this research was provided by grants from CONICET, Universidad Nacional del Sur and Agencia Nacional de Promoción Científica y Tecnológica (ANPCYT).

References

Belgiu, M., Csillik, O., 2018. Sentinel-2 cropland mapping using pixel-based and object-based time-weighted dynamic time warping analysis. Remote sensing of environment 204, 509–523.

Boston, K. G., 1983. The Development of Salt Pans on Tidal Marshes, with Particular Reference to South-Eastern Australia. Journal of Biogeography 10 (1), 1–10.

Brand, L. A., Smith, L. M., Takekawa, J. Y., Athearn, N. D., Taylor, K., Shellenbarger, G., Schoellhamer, D. H., Spenst, R., 2012. Trajectory of early tidal marsh restoration: Elevation, sedimentation and colonization of breached salt ponds in the northern San Francisco Bay. Ecological Engineering 42, 19–29.

Chapman, V. J. V. J., 1960. Salt marshes and salt deserts of the world. Interscience Publishers, London.

Cipolletti, M. P., Delrieux, C. A., Perillo, G. M. E., Piccolo, M. C., 2012. Superresolution border segmentation and measurement in remote sensing images. Computers & Geosciensces 40 (0), 87–96.

Cipolletti, M. P., Delrieux, C. A., Perillo, G. M. E., Piccolo, M. C., 2014. Border extrapolation using fractal attributes in remote sensing images. Computers & Geosciences 62, 25–34.

Cohen, J., 1960. A Coefficient of Agreement for Nominal Scales. Educational and Psychological Measurement 20 (1), 37–46.

Congalton, R. G., Green, K., 2008. Assessing the accuracy of remotely sensed data: principles and practices. CRC press.

Day, R., Quinn, G., 1989. Comparisons of treatments after an analysis of variance in ecology. Ecological monographs 59 (4), 433–463.

Escapa, M., Perillo, G. M. E., Iribarne, O., 2015. Biogeomorphically driven salt pan formation in Sarcocornia-dominated salt-marshes. Geomorphology 228, 147–157.

Feret, L. R., 1931. La grosseur des grains des matieres session pulverulentes. Association Internationale Pour Essai Des Materiaux 2 (1), 428–36.

Frey, R., 1985. Coastal and salt marshes. Coastal Sedimentary Environments, 187–224.

Ginsberg, S., Perillo, G. M. E., 2004. Characteristics of tidal channels in a mesotidal estuary of Argentina. Journal of Coastal Research, 489–497.

Gorelick, N., Hancher, M., Dixon, M., Ilyushchenko, S., Thau, D., Moore, R., 2017. Google earth engine: Planetary-scale geospatial analysis for everyone. Remote Sensing of Environment 202, 18–27.

Goudie, A., 2013. Characterising the distribution and morphology of creeks and pans on salt marshes in England and Wales using Google Earth. Estuarine, Coastal and Shelf Science 129, 112–123.

Ijaz, M. W., Mahar, R. B., Siyal, A. A., Anjum, M. N., 2018. Geospatial analysis of creeks evolution in the indus delta, pakistan using multi sensor satellite data. Estuarine, Coastal and Shelf Science 200, 324–334.

Melo, W. Piccolo, M. C., Perillo, G. M. E., 2006. Morfogenesis de las islas del estuario de Bah´ıa Blanca. Actas de la VI Jornadas Nacionales de Geografía Física 1 (1), 112–122.

Melo, W. D., 2004. Cuenca de Recepción del Estuario de Bahía Blanca. Ph.D. thesis, Departamento de Geografía, Universidad Nacional del Sur.

Packham, J, R., Liddle, M. J., 1970. The Cefni salt marsh, Anglesey, and its recent development. Field studies 3, 331–356.

Perillo, G. M. E., Piccolo, M. C., 1999. Geomorphological and physical characteristics of the Bahía Blanca Estuary, Argentina. In: Perillo, G. M. E., Piccolo, M. C. and Pino-Quivira, M. (Eds.). Estuaries of South America. Springer, pp. 195–216.

Perillo, G. M. E., 2009. Tidal courses: classification, origin and functionality. In: Perillo, G. M. E., Wolanski, E., Cahoon, D. R. and Brinson, M. M. (Eds). Coastal Wetlands: An Integrated Ecosystem Approach. Elsevier, Amsterdam, 185–209.

Perillo, G. M. E., 2019. Geomorphology of tidal courses and depressions. In: Perillo, G.M.E., Wolanski, E., Cahoon, D.R. and Hopkinson, C. (Eds.). Coastal wetlands: An Integrated Ecosystem Approach. Elsevier, Amsterdam, 221–261.

Perillo, G. M. E., Iribarne, O. O., 2003. New mechanisms studied for creek formation in tidal flats: From crabs to tidal channels. Eos, Transactions American Geophysical Union 84 (1), 1–5.

Perillo, G. M. E., Piccolo, M. C., 1991. Tidal response in the Bahía Blanca Estuary. Journal of Coastal Research 7 (2), 437–449.

Perillo, G. M. E., Piccolo, M. C., Parodi, E., Freije, R. H., 2001. The Bahia Blanca Estuary, Argentina. In: Seeliger, U., Kjerfve, B. (Eds.). Coastal Marine Ecosystems of Latin America 144. Springer, Berlin Heidelberg, pp. 205–217.

Pestrong, R., 1965. The development of drainage patterns on tidal marshes. Stanford University publications 10 (2).

Pethick, J. S., 1974. The Distribution of Salt Pans on Tidal Salt Marshes. Journal of Biogeography 1 (1), 57–62.

Piccolo, M. C., Capelli de Steffens, A., Campo de Ferreras, A., 1989. Variaciǿn espacial del viento en el Area de Bah´ıa Blanca. Revista Geof´ısica 31, 205–220.

Piccolo, M. C., Perillo, G. M. E., Melo, W., 2008. The Bah´ıa Blanca Estuary: an integrated overview of its geomorphology and dynamics. In: Neves, R., Baretta, J. and Mateus,
M. (Eds.). Perspectives on integrated coastal zone management in South America. IST Press, Lisboa. 1, 221–231.

Pontius, J., Robert, G., Millones, M., 2011. Death to Kappa: birth of quantity disagreement and allocation disagreement for accuracy assessment. International Journal of Remote Sensing 32 (15), 4407–4429.

Pratolongo, P., Perillo, G. M. E., Piccolo, M. C., 2010. Combined effects of waves and marsh plants on mud deposition events at a mudflat-saltmarsh edge. Estuarine, Coastal and Shelf Sciences 87, 207–212.

Revollo, N. V., Delrieux, C. A., Perillo, G. M. E., 2016. Automatic methodology for mapping of coastal zones in video sequences. Marine Geology 381, 87–101.

Revollo Sarmiento, G. N., Cipolletti, M. P., Perillo, M. M., Delrieux, C. A., Perillo, G. M. E., 2016. Methodology for classification of geographical features with remote sensing images: Application to tidal flats. Geomorphology 257, 10–22.

Rishikeshan, C., Ramesh, H., 2017. A novel mathematical morphology based algorithm for shoreline extraction from satellite images. Geo-spatial Information Science 20 (4), 345–352.

Russ, J. C., 1999. The Image Processing Handbook, 3rd Edition. CRC Press, Boca Raton, FL.

Shih, S., Hwang, G., Hsieh, H., Chen, C., Chen, Y., 2015. Geomorphologic dynamics and maintenance following mudflat, creek and pond formation in an estuarine mangrove wetland. Ecological Engineering 82, 590–595.

Steers, J. A., 1964. The coastline of England and Wales. Cambridge Univ. Press, Reidel, Dordrecht.

Tatar, N., Saadatseresht, M., Arefi, H., Hadavand, A., 2018. A robust object-based shadow detection method for cloud-free high resolution satellite images over urban areas and water bodies. Advances in Space Research 61 (11), 2787–2800.

Verger, F., 1968. Marais et wadden du littoral français: étude de géomorphologie.

Biscaye Freres.

Wang, W., Yan, X., Zhao, L., Shi, J., 2017. A new affine invariant descriptor for shape recognition. In: Jhon W and Sons (Eds.). Computer and Communications (ICCC), 2017 3rd IEEE International Conference on. IEEE, China, 1693–1697.

Wilkinson, G. G., 2005. Results and implications of a study of fifteen years of satellite image classification experiments. IEEE Transactions on Geoscience and remote sensing 43 (3), 433–440.

Yapp, R. H., Johns, D., Jones, O. T., 1917. The Salt Marshes of the Dovey Estuary. Journal of Ecology 5 (2), 65–103.

Zhang, T. Y., Suen, C. Y., 1984. A fast parallel algorithm for thinning digital patterns. Communications of the ACM 27 (3), 236–239.

Supplement

Classification results and performance matrix per site.

Site 1

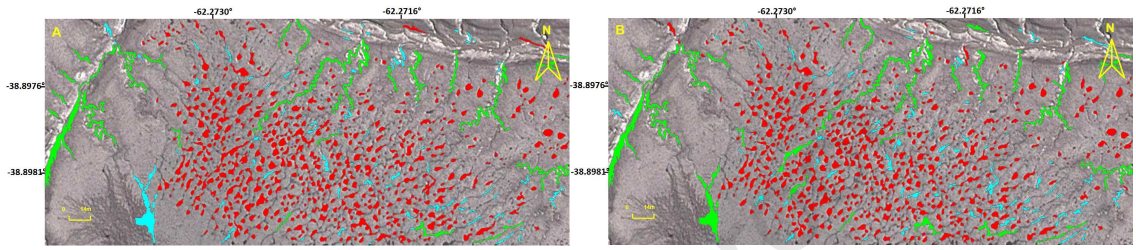

Fig. 12. Classification results in Bahía Blanca Estuary; site 1 with it global precision. (A) Supervised classification A_g = 100 %. (B) Automatic classification A_g = 90.6 %. Ponds, tidal channels and others are shown in red, green, and cyan, respectively.

Table 7. Performance matrix Site 1. (A) Confusion matrix. (B) Quality standard terms.

A

		Predicted		
		P	C	O
Actual	P	520	4	31
	C	0	27	1
	O	26	1	58

B

Parameter	Value
A_g[%]	90.57
$R_{T\,p}$	0.94
$R_{T\,c}$	0.96
$R_{T\,o}$	0.68
R_{Fp}	0.95
R_{Fc}	0.84
R_{Fo}	0.64
$P_r(a)$	0.90
$P_r(e)$	0.70
κ	0.69

Site 2

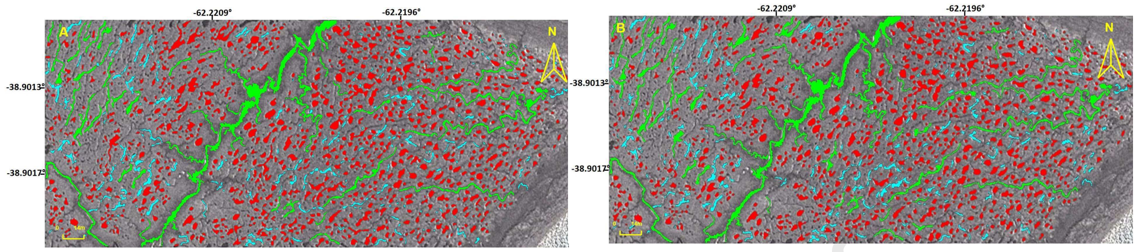

Fig. 13. Classification results in Bahía Blanca Estuary; site 2 with it global precision. (A) Supervised classification-A_g = 100 %. (B) Automatic classification -A_g = 86 %. Ponds, tidal channels and others are shown in red, green, and cyan, respectively.

Table 8. Performance matrix Site 2. (A) Confusion matrix. (B) Quality standard terms.

A

		Predicted		
		P	C	O
Actual	P	833	6	78
	C	1	37	0
	O	72	6	140

B

Parameter	Value
A_g[%]	86.10
$R_{T\,p}$	0.91
$R_{T\,c}$	0.97
$R_{T\,o}$	0.64
R_{Fp}	0.92
R_{Fc}	0.75
R_{Fo}	0.64
$P_r(a)$	0.86
$P_r(e)$	0.64
κ	0.61

Site 3

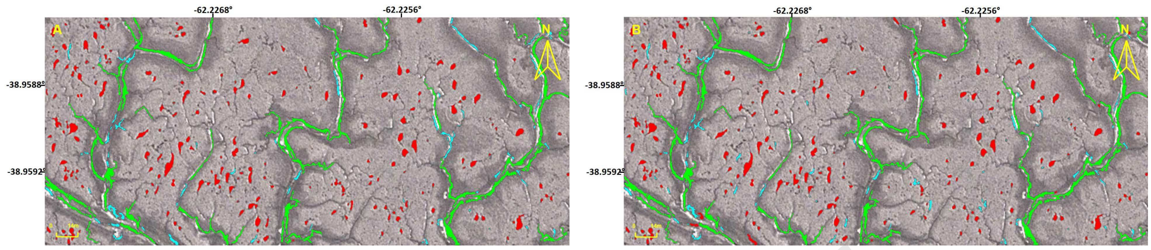

Fig. 14. Classification results in Bahía Blanca Estuary; site 3 with it global precision. (A) Supervised classification A_g = 100 %. (B) Automatic classification A_g = 89.5 %. Ponds, tidal channels and others are shown in red, green, and cyan, respectively.

Table 9. Performance matrix Site 3. (A) Confusion matrix. (B) Quality standard terms.

		A			B	
		Predicted			Parameter	Value
		P	C	O	A_g[%]	89.46
	P	183	0	20	R_{Tp}	0.90
Actual	C	0	37	0	R_{Tc}	1.00
	O	11	2	60	R_{To}	0.82
					R_{Fp}	0.94
					R_{Fc}	0.95
					R_{Fo}	0.75
					$P_r(a)$	0.89
					$P_r(e)$	0.47
					κ	0.80

Site 4

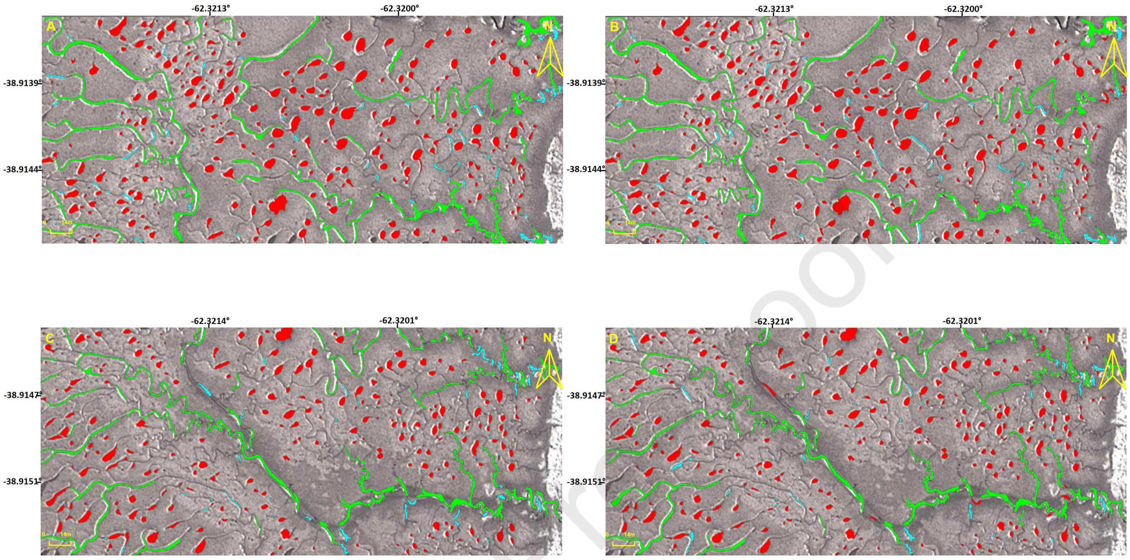

Fig. 15. Classification results in Bahía Blanca Estuary; site 4 with it global precision. (A) Supervised classification A_g = 100 %. (B) Automatic classification A_g = 92 %. (C) Supervised classification A_g = 100 %. (D) Automatic classification A_g = 90 %. Ponds, tidal channels and others are shown in red, green, and cyan, respectively.

Table 10. Performance matrix Site 4. (A) and (B): Confusion matrix and Quality standard terms site 4a. (C) and (D): Confusion matrix and Quality standard terms site 4b.

A

		Predicted		
		P	C	O
Actual	P	230	0	4
	C	0	29	3
	O	14	5	34

B

Parameter	Value
A_g[%]	91.85
$R_{T\,p}$	0.98
$R_{T\,c}$	0.90
$R_{T\,o}$	0.64
R_{Fp}	0.94
R_{Fc}	0.85
R_{Fo}	0.83
$P_r(a)$	0.92
$P_r(e)$	0.59
κ	0.80

C

		Predicted		
		P	C	O
Actual	P	208	1	9
	C	0	37	2
	O	15	2	26

D

Parameter	Value
A_g[%]	90.33
$R_{T\,p}$	0.95
$R_{T\,c}$	0.95
$R_{T\,o}$	0.60
R_{Fp}	0.93
R_{Fc}	0.92
R_{Fo}	0.70
$P_r(a)$	0.90
$P_r(e)$	0.57
κ	0.77

Site 5

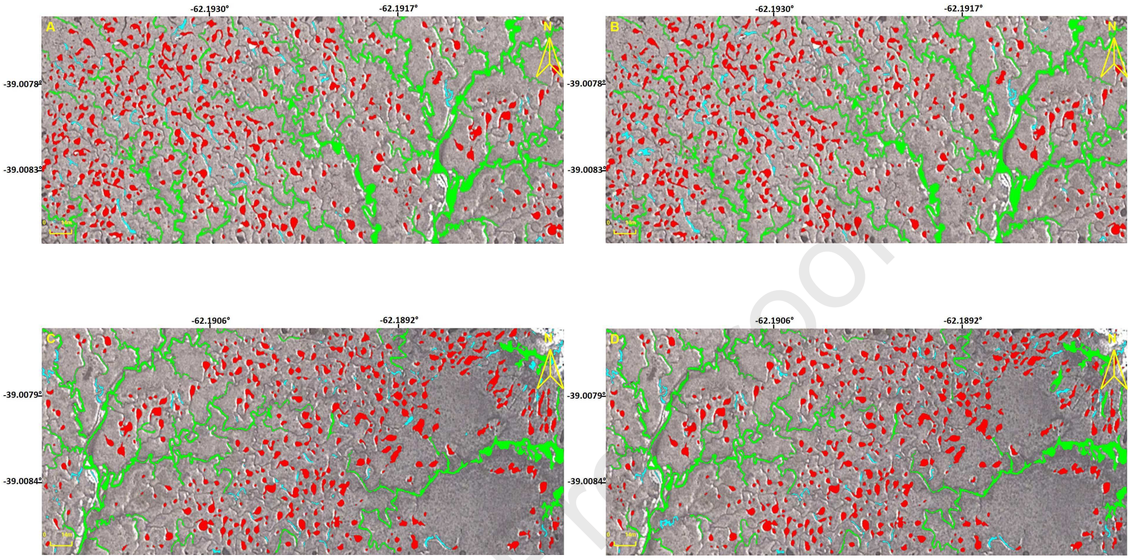

Fig. 16. Classification results in Bahía Blanca Estuary; site 5 with it global precision. (A) Supervised classification A_g = 100 %. (B) Automatic classification A_g = 92 %. (C) Supervised classification A_g = 100 %. (D) Automatic classification A_g = 91 %. Ponds, tidal channels and others are shown in red, green, and cyan, respectively.

Table 11. Performance matrix Site 5. (A) and (B): Confusion matrix and Quality standard terms in site 5a. (C) and (D): Confusion matrix and Quality standard terms in site 5b.

A

		Predicted P	Predicted C	Predicted O
Actual	P	473	0	31
	C	0	38	0
	O	17	2	63

B

Parameter	Value
A_g[%]	92
R_{Tp}	0.94
R_{Tc}	1.00
R_{To}	0.77
R_{Fp}	0.97
R_{Fc}	0.95
R_{Fo}	0.67
$P_r(a)$	0.92
$P_r(e)$	0.66
κ	0.77

C

		Predicted P	Predicted C	Predicted O
Actual	P	378	2	11
	C	0	38	1
	O	31	1	53

D

Parameter	Value
A_g[%]	91
R_{Tp}	0.97
R_{Tc}	0.97
R_{To}	0.62
R_{Fp}	0.92
R_{Fc}	0.93
R_{Fo}	0.82
$P_r(a)$	0.91
$P_r(e)$	0.63
κ	0.76

Site 6

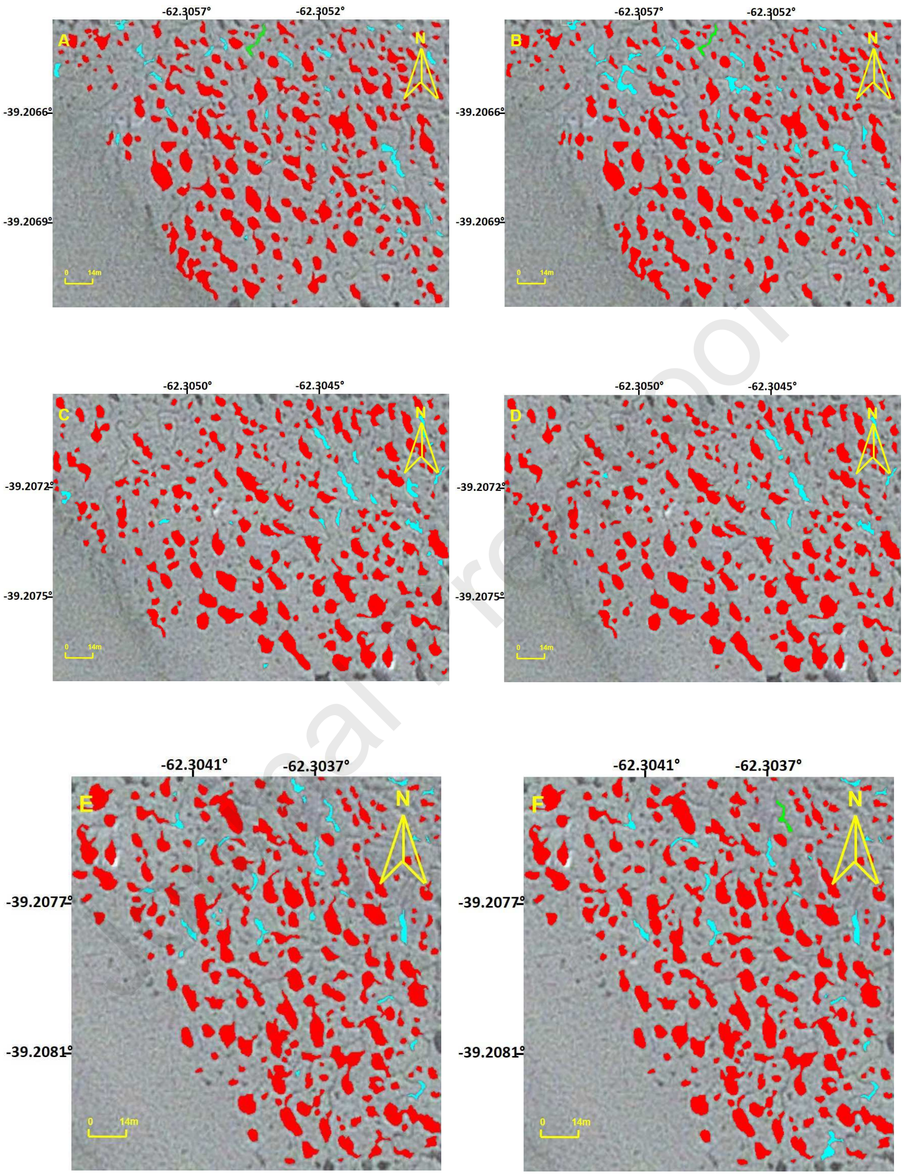

Fig. 17. Classification results in Bahía Blanca Estuary; site 6 with it global precision. (A) Supervised classification A_g = 100 %. (B) Automatic classification A_g = 94 %. (C) Supervised classification A_g = 100 %. (D) Automatic classification A_g = 94 %. (E) Supervised classification A_g = 100 %. (F) Automatic classification A_g = 92 %. Ponds, tidal channels and others are shown in red, green and cyan, respectively.

Table 12. Performance matrix Site 6. (A) and (B): Confusion matrix and Quality standard terms in site 6a. (C) and (D): Confusion matrix and Quality standard terms in site 6b.

A

		Predicted		
		P	C	O
Actual	P	227	0	8
	C	0	1	0
	O	8	0	20

B

Parameter	Value
A_g[%]	93.9
$R_{T\,p}$	0.97
$R_{T\,c}$	1.00
$R_{T\,o}$	0.71
R_{Fp}	0.97
R_{Fc}	1.00
R_{Fo}	0.71
$P_r(a)$	0.94
$P_r(e)$	0.80
κ	0.70

C

		Predicted		
		P	C	O
Actual	P	197	0	3
	C	0	0	0
	O	10	0	7

D

Parameter	Value
A_g[%]	94
$R_{T\,p}$	0.99
$R_{T\,c}$	*NaN*
$R_{T\,o}$	0.41
R_{Fp}	0.95
R_{Fc}	*NaN*
R_{Fo}	0.7
$P_r(a)$	0.94
$P_r(e)$	0.88
κ	0.5

Table 13. Performance matrix Site 6c. (A) Confusion matrix and (B) Quality standard terms.

		A			B	
		Predicted			Parameter	Value
		P	C	O	A_g[%]	92.2
Actual	P	186	0	4	R_{Tp}	0.98
	C	0	0	0	R_{Tc}	*NaN*
	O	12	1	16	R_{To}	0.55
					R_{Fp}	0.94
					R_{Fc}	0.00
					R_{Fo}	0.8
					$P_r(a)$	0.92
					$P_r(e)$	0.80
					κ	0.62

Site 7

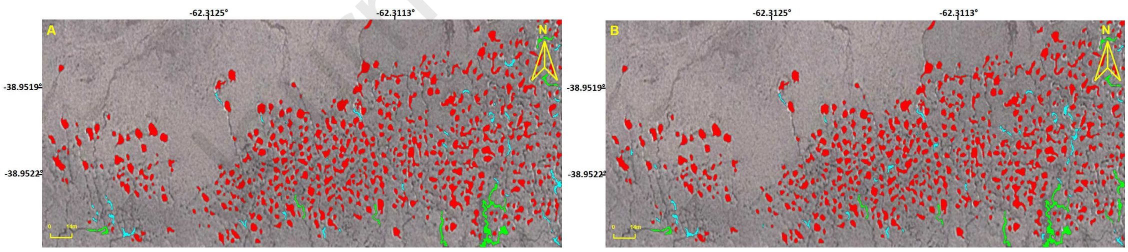

Fig. 18. Classification results in Bahía Blanca Estuary; site 7 with it global precision. (A) Supervised classification A_g = 100 %. (B) Automatic classification A_g = 95 %. Ponds, tidal channels and others are shown in red, green, and cyan, respectively.

Table 14. Performance matrix Site 7. (A) Confusion matrix and (B) Quality standard terms.

A

		Predicted		
		P	C	O
Actual	P	515	1	14
	C	0	7	0
	O	10	2	23

B

Parameter	Value
A_g[%]	95.28
$R_{T\,p}$	0.97
$R_{T\,c}$	1.00
$R_{T\,o}$	0.66
R_{Fp}	0.98
R_{Fc}	0.70
R_{Fo}	0.62
$P_r(a)$	0.95
$P_r(e)$	0.85
κ	0.67

Site 8

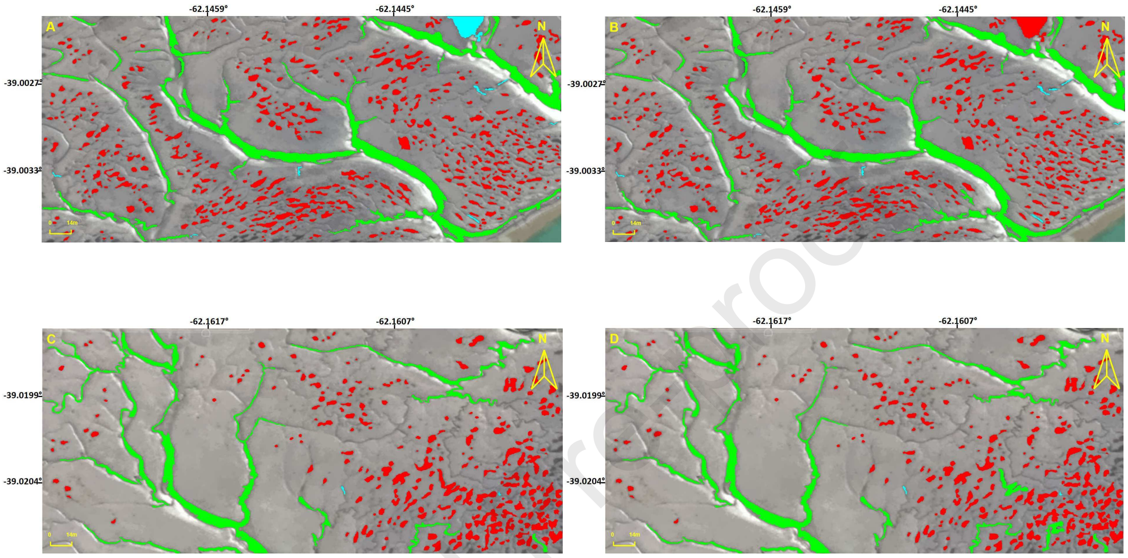

Fig. 19. Classification results in Bahía Blanca Estuary; site 8 with it global precision. (A) Supervised classification A_g = 100 %. (B) Automatic classification A_g = 99.4 %. (C) Supervised classification A_g = 100 %. (D) Automatic classification A_g = 99.2 %. Ponds, tidal channels and others are shown in red, green, and cyan, respectively.

Table 15. Performance matrix Site 8. (A) and (B): Confusion matrix and Quality standard terms site 8a. (C) and (D): Confusion matrix and Quality standard terms site 8b.

A

		Predicted		
		P	C	O
Actual	P	486	1	0
	C	0	25	0
	O	2	0	10

B

Parameter	Value
A_g[%]	99.4
R_{Tp}	0.99
R_{Tc}	1.00
R_{To}	0.83
R_{Fp}	0.99
R_{Fc}	0.96
R_{Fo}	1.00
$P_r(a)$	0.99
$P_r(e)$	0.87
κ	0.96

C

		Predicted		
		P	C	O
Actual	P	225	2	0
	C	0	12	0
	O	0	0	2

D

Parameter	Value
A_g[%]	99.2
R_{Tp}	0.99
R_{Tc}	1.00
R_{To}	1.00
R_{Fp}	1.00
R_{Fc}	0.86
R_{Fo}	1.00
$P_r(a)$	0.99
$P_r(e)$	0.88
κ	0.93

Site 9

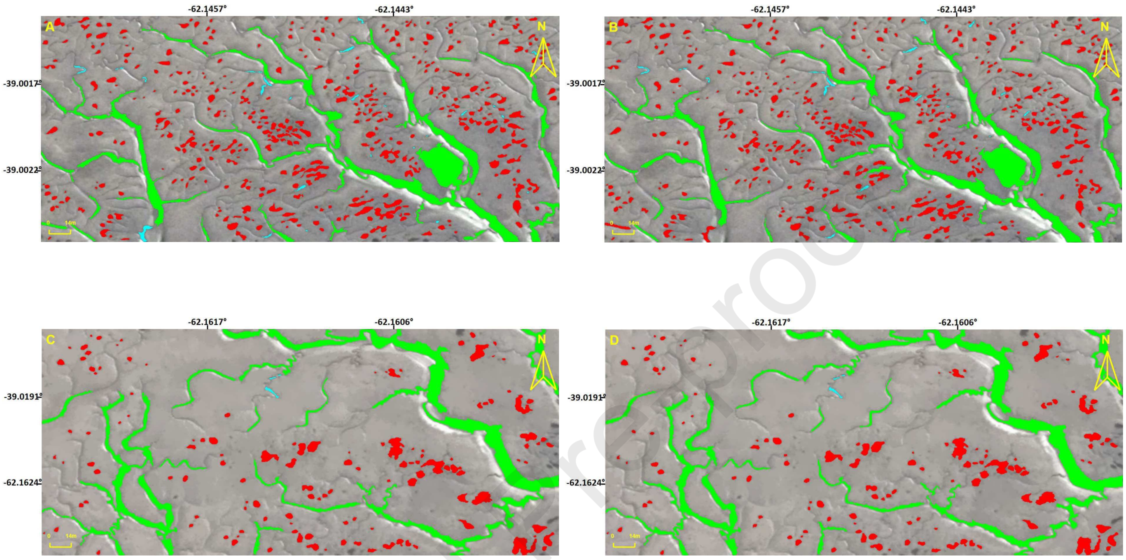

Fig. 20. Classification results in Bahía Blanca Estuary; site 9 with it global precision. (A) Supervised classification A_g = 100 %. (B) Automatic classification A_g = 97 %. (C) Supervised classification A_g = 100 %. (D) Automatic classification A_g= 100 %. Ponds, tidal channels and others are shown in red, green, and cyan, respectively.

Table 16. Performance matrix Site 9. (A) and (B): Confusion matrix and Quality standard terms site 9a. (C) and (D): Confusion matrix and Quality standard terms site 9b.

A

		Predicted		
		P	C	O
Actual	P	381	1	2
	C	1	27	0
	O	11	0	16

B

Parameter	Value
A_g[%]	96.6
$R_{T\,p}$	0.99
$R_{T\,c}$	0.96
$R_{T\,o}$	0.59
R_{Fp}	0.97
R_{Fc}	0.96
R_{Fo}	0.88
$P_r(a)$	0.96
$P_r(e)$	0.78
κ	0.84

C

		Predicted		
		P	C	O
Actual	P	126	0	0
	C	0	15	0
	O	0	0	4

D

Parameter	Value
A_g[%]	100
$R_{T\,p}$	1.00
$R_{T\,c}$	1.00
$R_{T\,o}$	1.00
R_{Fp}	1.00
R_{Fc}	1.00
R_{Fo}	1.00
$P_r(a)$	1.00
$P_r(e)$	0.77
κ	1.00

Site 10

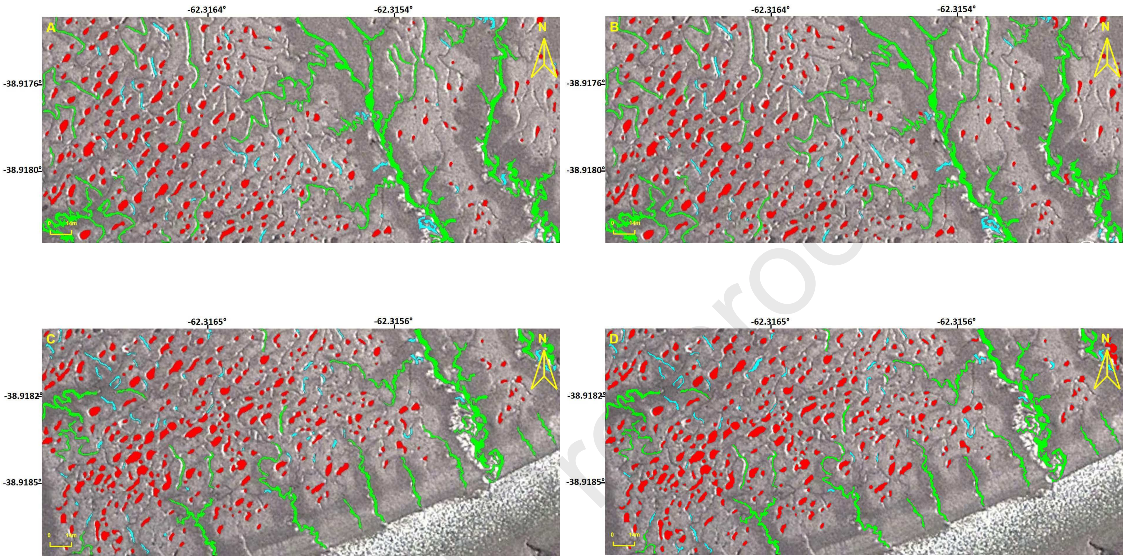

Fig. 21. Classification results in Bahía Blanca Estuary; site 10 with it global precision. (A) Supervised classification A_g = 100 %. (B) Automatic classification A_g = 96 %. (C) Supervised classification A_g = 100 %. (D) Automatic classification A_g = 94 %. Ponds, tidal channels and others are shown in red, green, and cyan, respectively.

Table 17. Performance matrix Site 10. (A) and (B): Confusion matrix and Quality standard terms site 10a. (C) and (D): Confusion matrix and Quality standard terms site 10b.

A

		Predicted		
		P	C	O
Actual	P	240	0	1
	C	0	31	0
	O	9	2	37

B

Parameter	Value
A_g[%]	96.2
$R_{T\,p}$	0.99
$R_{T\,c}$	1.00
$R_{T\,o}$	0.77
R_{Fp}	0.96
R_{Fc}	0.94
R_{Fo}	0.97
$P_r(a)$	0.96
$P_r(e)$	0.61
κ	0.90

C

		Predicted		
		P	C	O
Actual	P	275	0	5
	C	1	25	0
	O	14	1	42

D

Parameter	Value
A_g[%]	94.2
$R_{T\,p}$	0.98
$R_{T\,c}$	0.96
$R_{T\,o}$	0.74
R_{Fp}	0.95
R_{Fc}	0.96
R_{Fo}	0.89
$P_r(a)$	0.94
$P_r(e)$	0.64
κ	0.84

Site 11

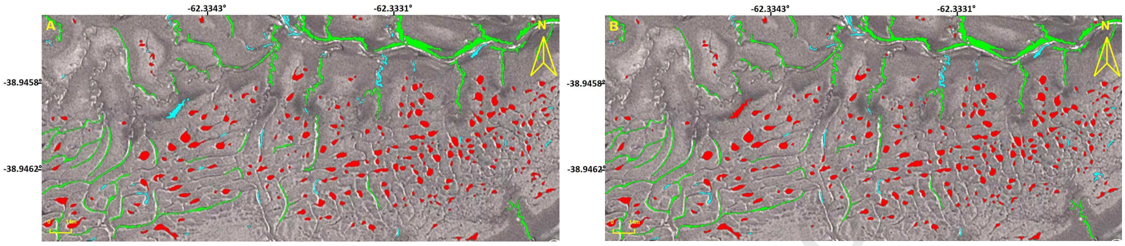

Fig. 22. Classification results in Bahía Blanca Estuary; site 11 with it global precision. (A) Supervised classification A_g = 100 %. (B) Automatic classification A_g = 95 %. Ponds, tidal channels and others are shown in red, green, and cyan, respectively.

Table 18. Performance matrix Site 11. (A) Confusion matrix and (B) Quality standard terms.

		A			B	
		Predicted			Parameter	Value
		P	C	O	A_g[%]	95.44
Actual	P	247	0	2	R_{Tp}	0.99
	C	0	37	0	R_{Tc}	1.00
	O	13	0	30	R_{To}	0.70
					R_{Fp}	0.95
					R_{Fc}	1.00
					R_{Fo}	0.94
					$P_r(a)$	0.95
					$P_r(e)$	0.62
					κ	0.88

Site 14

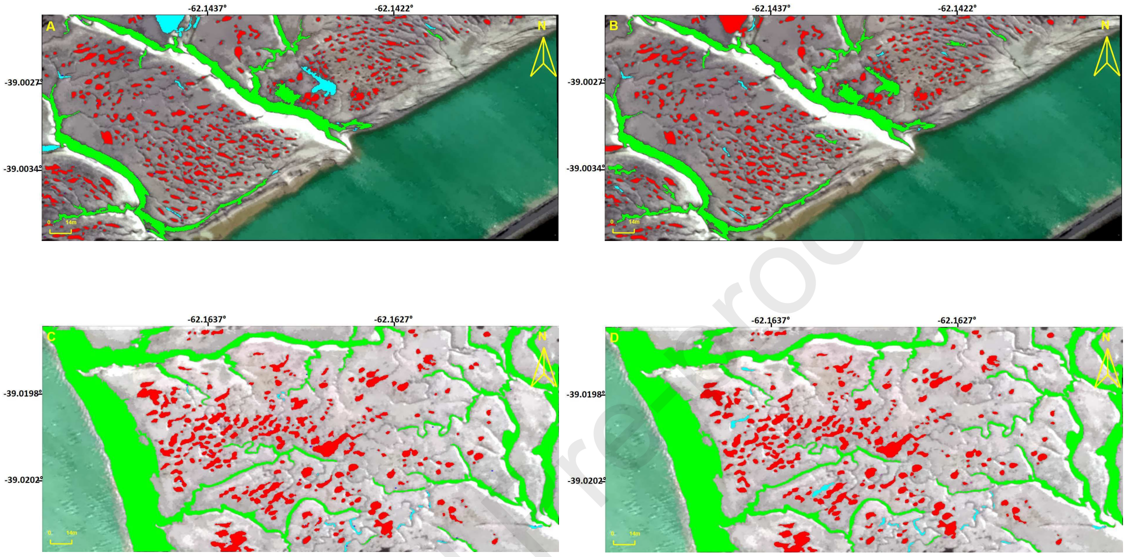

Fig. 23. Classification results in Bahía Blanca Estuary; site 14 with it global precision. (A) Supervised classification A_g = 100 %. (B) Automatic classification A_g = 96 %. (C) Supervised classification A_g = 100 %. (D) Automatic classification A_g = 96 %. Ponds, tidal channels and others are shown in red, green and cyan, respectively.

Table 19. Performance matrix Site 14. (A) and (B): Confusion matrix and Quality standard terms site 14a. (C) and (D): Confusion matrix and Quality standard terms site 14b.

A

		Predicted		
		P	C	O
Actual	P	383	5	5
	C	0	7	0
	O	6	1	5

B

Parameter	Value
A_g[%]	95.87
R_{Tp}	0.97
R_{Tc}	1.00
R_{To}	0.42
R_{Fp}	0.98
R_{Fc}	0.53
R_{Fo}	0.5
$P_r(a)$	0.95
$P_r(e)$	0.90
κ	0.57

C

		Predicted		
		P	C	O
Actual	P	214	0	5
	C	0	9	0
	O	4	0	11

D

Parameter	Value
A_g[%]	96.3
R_{Tp}	0.98
R_{Tc}	1.00
R_{To}	0.73
R_{Fp}	0.98
R_{Fc}	1.00
R_{Fo}	0.68
$P_r(a)$	0.96
$P_r(e)$	0.81
κ	0.80

Author Statement

Revollo Sarmiento, Gisela Noelia: Conceptualization, Methodology, Software, Writing.

Revollo Natalia.: Processing image, Writing.

Delrieux, Claudio: Supervision, Writing.

Perillo, Gerardo M. E.*:* Supervision, Data Analysis.

Declaration of interests

☒ The authors declare that they have no known competing financial interests or personal relationships that could have appeared to influence the work reported in this paper.

☒The authors declare the following financial interests/personal relationships which may be considered as potential competing interests:

Partial financial support for this research was provided by grants from CONICET, Universidad Nacional del Sur and Agencia Nacional de Promoción Científica y Tecnológica (ANPCYT).